Lithos 274–275 (2017) 291–303

Contents lists available at ScienceDirect

Lithos

journal homepage: www.elsevier.com/locate/lithos

Oceanic mafic magmatism in the Siletz terrane, NW North America: Fragments of an Eocene oceanic plateau?

Bethan A. Phillips [a,*], Andrew C. Kerr [a], Emily K. Mullen [b], Dominique Weis [b]

[a] School of Earth and Ocean Sciences, Cardiff University, Park Place, Cardiff CF10 3AT, UK
[b] Pacific Centre for Isotopic and Geochemical Research, Department of Earth, Ocean and Atmospheric Sciences, University of British Columbia, Vancouver, BC V6T 1Z4, Canada

ARTICLE INFO

Article history:
Received 11 October 2016
Accepted 5 January 2017
Available online 14 January 2017

Keywords:
Oceanic plateau
Siletz terrane
Large igneous province
NW United Sates
Mantle plume

ABSTRACT

The Siletz terrane, a predominantly mafic accreted oceanic terrane, is located in the Cascadia forearc region of Oregon, Washington and Vancouver Island. The terrane represents a late Palaeocene–Eocene large igneous province that consists of pillow lavas, massive flows and intrusive sheets. Previously it has been proposed that the Siletz terrane represents either an accreted oceanic plateau, hotspot island chain, backarc basin, island arc, or a sequence of slab window volcanics. A province-wide geochemical reassessment of the terrane, including new high precision Sr-Pb-Nd-Hf isotope data, has been used to assess the validity of the proposed tectonomagmatic models for the Siletz terrane. The trace element data show little evidence of crustal contamination, or an arc signature, and the samples have rare earth element (REE) patterns that are flat to light REE enriched. These features are similar to other oceanic plateaus such as the Ontong Java and the Caribbean. Initial isotope ratios range from $^{206}Pb/^{204}$ Pb: 18.751 to 19.668, $^{207}Pb/^{204}Pb$: 15.507 to 15.661, $^{208}Pb/^{204}Pb$: 38.294 to 39.2128, $^{176}Hf/^{177}Hf$: 0.28300 to 0.28316 (ε_{Hf}: 9.0 to 14.5), $^{143}Nd/^{144}Nd$: 0.51282 to 0.51299 (ε_{Nd}: 5.0 to 8.1) and $^{87}Sr/^{86}Sr$: 0.70302 to 0.70380. These data are consistent with a mantle source of the Siletz terrane that appears to have been heterogeneous and slightly enriched. The enriched signature has characteristics of both EM2 and HIMU components and this, combined with a calculated mantle potential temperature well above ambient mantle, indicates derivation of the Siletz magmatism from a mantle plume, possibly the Yellowstone Hotspot. We therefore conclude that the Siletz terrane represents an accreted oceanic plateau.

1. Introduction

Accreted oceanic mafic terranes are an ubiquitous feature not only of most destructive plate margins (e.g., the northern Andes, (Kerr et al., 2002a); the coastal ranges of western Canada and Alaska (Greene et al., 2009a, 2009b), and Japan (e.g.,Ichiyama et al., 2014)), but also of continental collision zones such as that represented by the closure of the Tethyan ocean (e.g., Turkey (Whattam and Stern, 2011); Tibet (Chen et al., 2001); and central Iran (Moghadam et al., 2010)). Such mafic accreted terranes are common throughout most of Earths' history (e.g., Kerr, 2014) and so may have also contributed significantly to the growth of continental crust (Condie, 1998; Stern and Scholl, 2010). Many accreted oceanic mafic rocks represent areas of over-thickened (>6–7 km) oceanic crust (such as seamounts, ocean islands, aseismic ridges or oceanic plateaus) that was too buoyant to subduct (Cloos, 1993; Tetreault and Buiter, 2014). This uplifted and accreted oceanic crust affords an excellent opportunity to study the structure, composition and origin of a part of the ocean floor that would otherwise be relatively inaccessible.

This study focuses on the Siletz terrane, a mostly Eocene large igneous province (LIP) located in the present Cascadia forearc region of Oregon, Washington and Vancouver Island (Fig. 1), consisting of a series of accreted basaltic pillow lavas, massive flows and intrusive sheets (Snavely et al., 1968; Wells et al., 2014). The terrane is composed of both subaerial and submarine rocks, with an estimated magmatic volume of 2.6×10^6 km^3 (Trehu et al., 1994). Eruption and intrusion of the Siletz terrane magmas are thought to have taken place from ~56 to 49 Ma (Duncan, 1982; Haeussler et al., 2000; Hirsch and Babcock, 2009; Massey, 1986; Wells et al., 2014) during a time of major plate reorganisation in the Pacific (Atwater, 1989; Engebretson, 1985). The terrane was rotated during accretion, shortly after formation within 300 km of the North American Pacific continental margin (McCrory and Wilson, 2013). The province has been variously known as: Siletzia (Irving, 1979), the Coast Range Volcanic Province (Babcock et al., 1992), the Siletz–Crescent terrane (McCrory and Wilson, 2013) and the Siletz terrane (Fleming and Trehu, 1999; Snavely et al., 1968) used in this paper.

At present, there is little consensus on the tectonic setting in which the Siletz terrane magmas were generated. Previously proposed models include initial melting of the Yellowstone mantle plume head (Pyle et al., 2009; Wells et al., 2014), accretion of a hotspot island chain

* Corresponding author.
E-mail address: phillipsba@cardiff.ac.uk (B.A. Phillips).

http://dx.doi.org/10.1016/j.lithos.2017.01.005

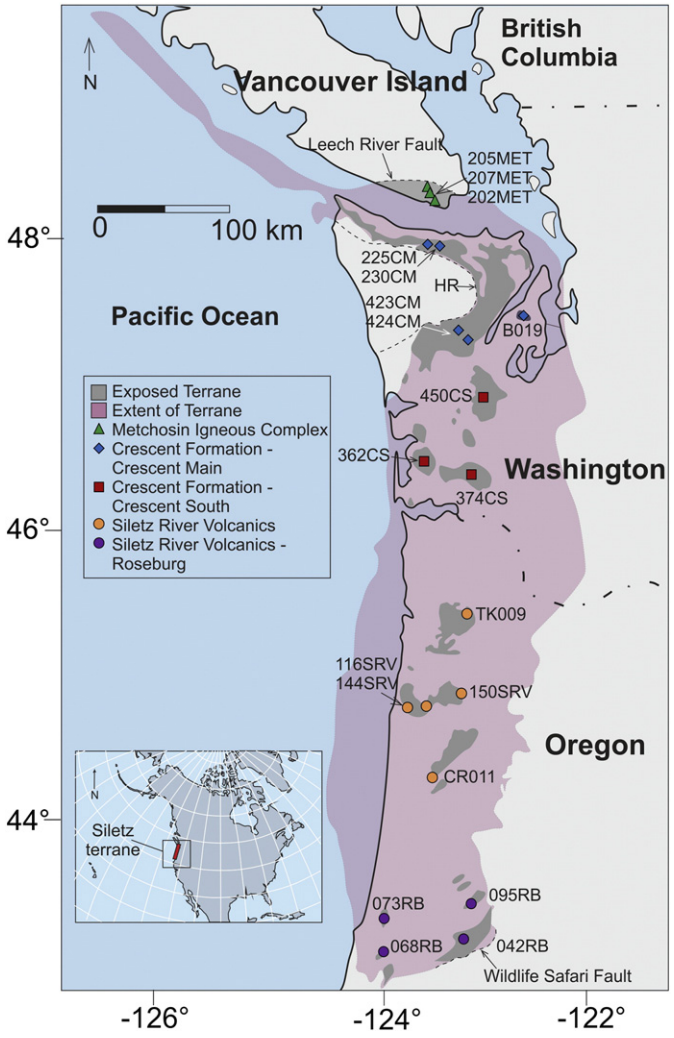

Fig. 1. Map of the extent and exposed areas of the Siletz Terrane, adapted from McCrory and Wilson (2013). HR – Hurricane Ridge Fault.

(Duncan, 1982; McCrory and Wilson, 2013), Kula ridge subduction producing marginal rifting (Massey, 1986; Wells et al., 1984) and formation in a slab window-related setting (Babcock et al., 1992; Breitsprecher et al., 2003; Groome et al., 2003; Haeussler et al., 2003). In this paper we present a province-wide geochemical reassessment of the terrane, including new high precision Sr-Pb-Nd-Hf isotope data on 20 basaltic and gabbroic samples. The primary goals of this investigation are to use these new geochemical data to assess the nature of the mantle source region and the validity of the proposed tectonomagmatic models for the Siletz terrane.

2. Geological history and tectonic setting

The ~650 km-long Siletz Terrane consists of three main volcanic formations: the Siletz River Volcanics in Oregon, the Crescent Formation in southwestern Washington and the Olympic Peninsula, and the Metchosin Igneous Complex on the southeastern coast of Vancouver Island (Fig. 1). Although exposure is generally poor across most of the Siletz terrane, it is clear that the lower part of the terrane sequence contains mostly submarine pillow basalts, pillow breccia, gabbros and occasional sheeted dyke units (Duncan, 1982; Haeussler et al., 2000; Massey, 1986; Snavely et al., 1968; Wells et al., 2000). The upper part of the sequence contains both submarine pillow basalts and subaerial massive flows with oxidised flow tops along with rare felsic flows (Duncan, 1982; Haeussler et al., 2000; Massey, 1986; Snavely et al., 1968; Wells et al., 2000). These subaerial units are interbedded with brecciated lapilli tuffs, laminated tuffs and volcaniclastic sediments. The thickest part of the terrane occurs in central Oregon, where it reaches 27 ± 5 km (Trehu et al., 1994). Beneath northwestern Oregon and southwestern Washington, the terrane is approximately 20 km thick (Parsons et al., 1999), thinning to 10 km in northwestern Washington and southwestern Vancouver Island and down to 6 km offshore Vancouver Island (Hyndman et al., 1990).

The western boundary of the terrane is poorly exposed at the Hurricane Ridge fault (Fig. 1) on the Olympic Peninsula, Washington (Cady, 1975; Hirsch and Babcock, 2009). Using magnetic anomalies this boundary has been traced southwards (offshore Oregon) and northwards (off the coast of Vancouver Island) (Fig. 1) (Fleming and Trehu, 1999; Snavely et al., 1980). In the north, the Leech River Fault, a thrust contact on Vancouver Island, represents the eastern boundary of the terrane (Massey, 1986) while another thrust contact (Wildlife Safari fault) near Roseburg, Oregon, defines the eastern boundary in the south of the terrane (Wells et al., 2000) (Fig. 1). The southern margin of the Yakutat terrane in Alaska (Davis and Plafker, 1986) and the Wheatfield Fork Terrane of the Franciscan Complex in Northern California (McLaughlin, 2009) have also been proposed to be remnants of the Siletz terrane.

The age of the Siletz terrane has generally been constrained using ^{40}Ar-^{39}Ar whole rock dating techniques, placing the maximum age range of the terrane between 56 and 49 Ma, with the majority of the terrane having erupted between 54 and 50 Ma (Brandon, 2014; Duncan, 1982; Pyle et al., 2009). Nanoplankton ages from interbedded sediments have also been correlated by Wells et al. (2014) with other ages from across the terrane. In addition to this, limited U–Pb ages have also been determined. Haeussler et al. (2000) reported a U–Pb zircon age of 50.5 Ma for the Bremerton Igneous Complex in the Crescent Formation and U–Pb zircon ages of 52 and 54 Ma have been determined for the volcanics of the Metchosin Igneous Complex by Yorath et al. (1999). Several areas of the terrane have not been dated, resulting in some uncertainties in the relative timing of magmatism across the terrane. In addition, correlating the stratigraphy of different units across the terrane has proven difficult due to the lack of exposure.

Accretion is thought to have occurred rapidly after, and probably even during, the eruption of the terrane, first in the south between 51 and 49 Ma (Wells et al., 2014) and subsequently in the north from 48 Ma to 45 Ma (McCrory and Wilson, 2013; Wells et al., 2014). Accretion of the Siletz terrane may have triggered the break-up of the subducting Farallon slab and back-stepping of the subduction zone to the west of the accreted Siletz terrane (Gao et al., 2011).

It has been proposed that at the time of formation (Early Eocene) there were 4 (or 5) plates in the region; the Farallon, Kula, Pacific, North American (and Resurrection) plates (Fig. 2) (Haeussler et al., 2003; Seton et al., 2012). During this time a major change in the plate configuration took place, which resulted in an adjustment in spreading direction between the Pacific and Farallon plates from WSW–ENE to E–W (Atwater, 1989). The Pacific-Kula ridge also underwent a change in spreading direction from N–S to NW–SE (Seton et al., 2012) before an eventual cessation of spreading (Engebretson, 1985). Most early Eocene plate reconstruction models agree that the Farallon–Kula ridge was striking NE–SW at the time of formation of the Siletz terrane, intersecting the North American plate to the east, forming a triple junction with the Pacific plate in the west and a slab window at the adjacent margin of the North American continent (Atwater, 1989; Breitsprecher et al., 2003; Engebretson, 1985; Madsen et al., 2006; Seton et al., 2012).

The existence of an additional Resurrection plate between the Kula plate and the North American plate, to the north of the Farallon plate, has been proposed to account for the migration of magmatism along the southern margin of Alaska during the late Palaeocene to early Eocene (Haeussler et al., 2003). The Kula-Resurrection ridge has been modelled to have been subducted by 50 Ma (Breitsprecher et al.,

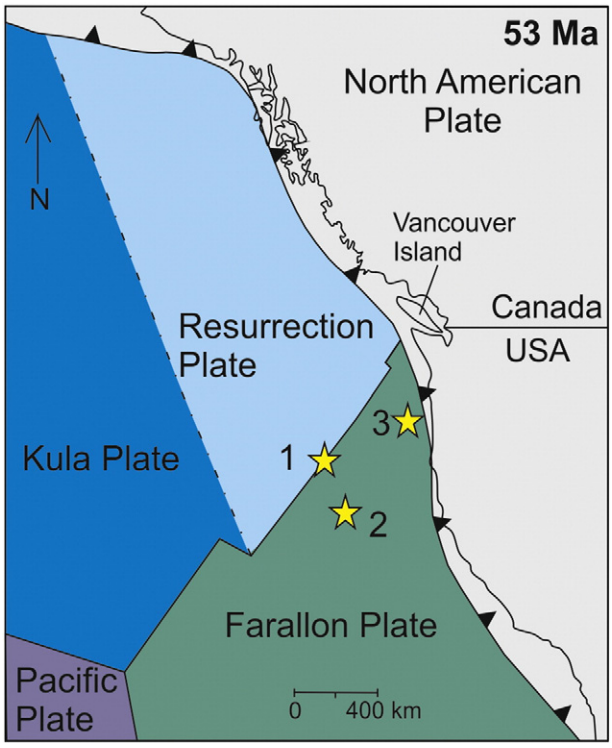

Fig. 2. Suggested plate configuration map at 53 Ma. Adapted from Haeussler et al. (2003), Seton et al. (2012) and Wells et al. (2014), where the stars represent the proposed positions of the Yellowstone hotspot; 1 (O'Neill et al. (2005), 2 (Doubrovine et al., 2012) and 3 (Müller et al., 1993).

2003; Haeussler et al., 2003; Wells et al., 2014) and the Siletz terrane is suggested to have formed on, or adjacent to, the mid-ocean ridge located between the Resurrection plate and the Farallon plate (McCrory and Wilson, 2013). It has also been argued that at this time (and at least since 60 Ma) the Yellowstone hotspot was located offshore of the North American continent; however, its location remains unclear (McCrory and Wilson, 2013). O'Neill et al. (2005) proposed that at 55 Ma the Yellowstone hotspot was located on the Kula–Farallon or Farallon–Resurrection ridge. Alternatively, Doubrovine et al. (2012) suggested that the hotspot was located off-axis on the Farallon plate whereas Müller et al. (1993) argued that it was adjacent to the North American continent and had moved underneath it by 50 Ma.

As discussed above, several models have been suggested to explain the geochemistry of the mantle source of the Siletz terrane and, as a result, a wide range of geochemical characteristics have been proposed for the mantle source of the terrane. Duncan (1982) suggested that the terrane represented a single accreted island chain formed by hotspot volcanism centred beneath the Kula–Farallon spreading ridge. Haeussler et al. (2003) further developed this model and proposed that the terrane comprises several composite terranes which represent two Yellowstone hotspot traces formed at the Resurrection-Farallon ridge and the Kula–Farallon ridge. A more recent model has proposed that the Siletz terrane formed on the Farallon plate and a sister terrane, the Yakutat terrane, erupted on the Kula (or Resurrection) plate as the Yellowstone hotspot interacted with the several ridges located in this region in the early Eocene (Wells et al., 2014). Pyle et al. (2009) suggested that the melting of the plume head phase of the Yellowstone hotspot was the dominant mechanism of formation. Other alternative models include formation in a marginal basin which was formed by oblique rifting of the continental margin (Brandon, 2014; Wells et al., 1984), or that the magmatism of the Siletz terrane was generated in a slab-window setting related to the subduction of a mid-ocean ridge (e.g., Babcock et al., 1992).

3. Petrography and sample locations

The terrane comprises vesicular basalts, dolerites, and gabbros, with occasional rhyolites and leucogabbros (a representative selection of photomicrographs can be found in Supplementary Material 1). The mafic rocks consist mostly of plagioclase, clinopyroxene and Fe–Ti oxide. Sub-ophitic textures in the plagioclase and clinopyroxene are common across the samples and zeolite-filled amygdales are abundant. Several samples collected from the Siletz River Volcanics also contain olivine in addition to the minerals noted above. The basalts and dolerites vary from phyric to aphyric, with the phyric samples containing up to ~20% plagioclase and clinopyroxene phenocrysts. Glomerocrysts of clinopyroxene and plagioclase are also common in the Crescent Formation and sections of the Siletz River Volcanics. Opaque phases predominantly consist of skeletal ulvospinel and ilmenite. Opaque minerals comprise between 10% and 20% of most samples and are particularly abundant in the Siletz River Volcanics (Roseburg).

The Metchosin Igneous Complex and some Crescent Formation samples display greenschist-facies alteration with chlorite, albite and epidote. Other Crescent Formation samples, and the Siletz River Volcanics to the south, have undergone zeolite to prehnite–pumpellyite facies alteration and contain zeolite, calcite, pumpellyite and prehnite. Palagonite is also a common alteration phase throughout the Siletz terrane samples and is interpreted to represent altered volcanic glass. Broad locations of the samples analysed for isotopic ratios are shown in Fig. 1 with precise locations given in Supplementary Material 2.

4. Analytical methods

4.1. Major and trace elements

Following removal of weathered surfaces by saw the samples were crushed in a steel jaw crusher and powdered using an agate Tema® mill at Cardiff University, Wales. Samples were then digested by fusion in platinum crucibles on a Claisse Fluxy automated fusion system using 0.1 ± 0.0005 g of sample with 0.4 ± 0.0005 g of lithium tetraborate flux (full methods described by McDonald and Viljoen (2006)). Major element abundances were analysed using a JY Horiba Ultima 2 inductively coupled plasma optical emission spectrometer (ICP-OES) and trace element abundances using a Thermo X7 series inductively coupled plasma mass spectrometer (ICP-MS) at Cardiff University. Accuracy and precision of the data were assessed using the international reference material JB-1A, which was run with each sample batch (Supplementary Material 3). The vast majority of elements are within 2 σ of certified values and those that are not in this range are not included.

4.2. Sr-Nd-Hf-Pb radiogenic isotopes

Twenty samples were selected for radiogenic isotope analyses based on lack of alteration, geographical spread and geochemical variability for a range of coverage. Chemical separations and mass spectrometric analyses were conducted in Class 100 laminar flow hoods in the Class 1000 clean laboratories at the Pacific Centre for Isotope and Geochemical Research at the University of British Columbia. Leaching was carried out prior to digestion as most samples show prehnite-pumpellyite to greenschist grade alteration and have LOI values between 0.5 and 2.0%. The leaching procedures are described in Nobre Silva et al. (2009). For each sample around 250 mg of rock powder was digested in sub-boiled HF and HNO_3 in 15 ml savillex beakers on a hotplate for around 48 h at 130 °C. The samples were subsequently dried down, 6 N HCl added and fluxed for 24 h, as outlined in Weis et al. (2006). Pb, Sr, Hf and Nd were separated from single powder dissolutions by sequential ion exchange column chemistry, having passed through the Pb columns twice to ensure purity (Weis et al., 2006, 2007). Pb, Hf, and Nd isotopic ratios

were measured on a Nu Plasma MC-ICP-MS 1700 or Nu Plasma II MC-ICP-MS instrument and Sr isotopic ratios were measured on a Triton TIMS instrument following procedures described by Weis et al. (2006). Full procedural blanks gave Sr, Nd, Hf and Pb concentrations of: Pb: 23.4 pg; Hf: 4–5 pg; Sr: 0.2–0.6 pg and Nd: 53–495 pg, which are negligible relative to sample concentrations.

5. Geochemical results

5.1. Major and trace elements

A representative dataset of the samples analysed for isotopes can be found in Table 1 and the full dataset in the Supplementary Material 4. The silica content of the analysed samples varies between 39.7 and 74.6 wt.% with the majority of samples having <50 wt.% SiO_2, while the Mg# varies between 18.5 and 70.8. The Cr abundance varies between 3.4 and 576 ppm and the Ni ranges between 3.1 and 1244 ppm. The LOIs of the samples are mostly between 0.5 and 2% but extend up to ~6%, which, along with the petrography, indicates that varying degrees of alteration have affected the rocks of the Siletz terrane. Under such conditions many elements, in particular the large-ion lithophile elements (i.e., K_2O, Ba, Rb), may become mobile (e.g., Hastie et al., 2007; Pearce, 1996).

Accordingly, these elements may not be representative of the original magmatic abundances in the rocks. The samples have therefore been classified using the Zr/Ti vs. Nb/Y diagram (Pearce, 1996), which utilises some of the relatively immobile high field strength elements (Fig. 2). On this classification diagram it can be seen that the majority of samples in this study are tholeiitic basalts while a small number of samples, largely from the Siletz River Volcanics, trend towards alkaline compositions (Fig. 3). This classification is generally in broad agreement with the major element data, with the majority of samples falling in a range of 44–52 SiO_2 wt.%, although there is more variability in the alkali oxides (K_2O + NaO) (alkali-silica diagram shown in Supplementary Material 5), than reflected in Fig. 3.

In Fig. 4 representative trace elements and ratios are plotted against Zr as it is relatively immobile and incompatible over the range of observed compositions (Cann, 1970). Many of the more immobile elements such as Nb, Th and La generally show a positive correlation with Zr (Fig. 3), and so are a more robust representation of the original magmatic variations among the rocks. The scatter observed on the diagrams in Fig. 4 is therefore unlikely to be related to alteration but due to variation in magmatic composition such

Table 1
Representative major and trace element data.

Sample #	225CM	423CM	B019	450CS	374CS	205MET	202MET	073RB	116SRV	144SRV
SiO_2	51.31	49.06	49.14	48.37	47.71	47.61	48.94	45.92	47.64	47.83
TiO_2	1.09	1.59	1.37	2.39	2.86	0.96	1.32	1.92	2.23	1.91
Al_2O_3	14.17	14.98	14.32	14.46	14.77	17.17	14.41	17.26	15.29	15.36
FeO*	12.73	11.88	10.92	13.40	15.05	11.58	13.32	13.15	13.12	13.78
MnO	0.19	0.17	0.10	0.25	0.25	0.21	0.20	0.22	0.31	0.24
MgO	7.25	7.85	7.55	6.22	4.65	8.06	6.76	7.40	7.15	5.64
CaO	10.09	11.71	14.23	11.91	11.58	12.79	11.81	9.88	11.64	12.37
Na_2O	2.82	2.18	2.11	2.43	2.51	1.46	3.09	2.90	2.18	2.43
K_2O	0.25	0.42	0.10	0.28	0.32	0.04	0.05	0.99	0.26	0.18
P_2O_5	0.10	0.16	0.16	0.26	0.27	0.09	0.11	0.34	0.19	0.25
LOI	1.29	1.11	1.90	1.01	1.54	1.11	1.68	0.95	1.39	0.12
Total (ppm)	99.83	100.67	99.80	99.53	99.15	99.63	98.60	100.25	99.89	97.31
Sc	47	46	46	42	40	41	47	25	40	46
V	375	308	nda	350	403	262	334	227	313	377
Cr	136	313	363	147	118	250	138	116	212	197
Co	46	45	51	61	41	43	47	49	51	52
Ni	109	116	111	122	133	171	80	45	85	74
Cu	106	63	153	158	177	108	118	53	98	105
Zn	102	107	70	114	144	96	57	83	118	118
Rb	0.94	1.34	5.52	2.22	3.14	0.24	1.29	4.98	0.68	0.20
Sr	91	323	231	269	250	100	116	652	222	232
Y	32.2	24.3	20.9	35.6	40.3	22.4	33.1	30.2	22.6	37.1
Zr	79	100	81	214	226	56	93	168	110	127
Nb	3.91	8.95	6.31	14.89	15.47	2.42	3.72	81.93	10.29	8.59
Ba	19	62	65	71	74	10	8	432	45	38
La	3.10	6.74	6.40	13.24	13.61	2.87	2.99	54.14	8.48	10.28
Ce	8.77	17.21	15.39	30.98	31.80	6.26	9.97	94.02	20.87	26.95
Pr	1.44	2.55	2.00	4.64	4.84	1.04	1.67	9.69	3.04	4.00
Nd	7.38	11.83	9.24	19.29	20.10	6.07	8.49	31.84	13.71	18.44
Sm	2.71	3.51	2.60	6.28	6.91	2.27	3.27	5.54	3.83	5.45
Eu	0.93	1.21	1.01	2.02	2.24	0.90	1.22	1.75	1.33	1.78
Gd	3.76	4.07	3.37	6.58	7.36	2.91	4.26	5.51	4.07	6.19
Tb	0.71	0.66	0.52	1.09	1.22	0.53	0.82	0.80	0.65	1.02
Dy	4.99	4.29	3.29	6.69	7.68	3.70	5.43	5.10	4.04	6.58
Ho	1.00	0.80	0.70	1.19	1.38	0.75	1.11	0.95	0.74	1.20
Er	3.01	2.23	2.03	3.46	4.16	2.28	3.37	2.77	1.99	3.41
Tm	0.52	0.36	0.31	0.52	0.63	0.38	0.55	0.46	0.32	0.54
Yb	3.32	2.25	1.85	3.19	3.74	2.29	3.51	3.03	1.95	3.45
Lu	0.53	0.32	0.29	0.46	0.55	0.34	0.53	0.45	0.28	0.54
Hf	1.93	2.40	2.10	5.07	5.62	1.44	2.39	3.13	2.62	3.13
Ta	0.22	0.48	0.36	0.99	1.04	0.15	0.20	4.51	0.63	0.71
Pb	5.21	3.08	2.16	0.66	2.96	0.17	1.03	4.02	7.41	3.41
Th	0.24	0.59	0.55	0.95	1.24	0.13	0.22	5.77	0.67	0.86
U	0.09	0.52	0.14	0.31	0.33	0.06	0.07	1.37	0.22	0.30

* Denotes total Iron. ** Total recalculated to an anhydrous basis.

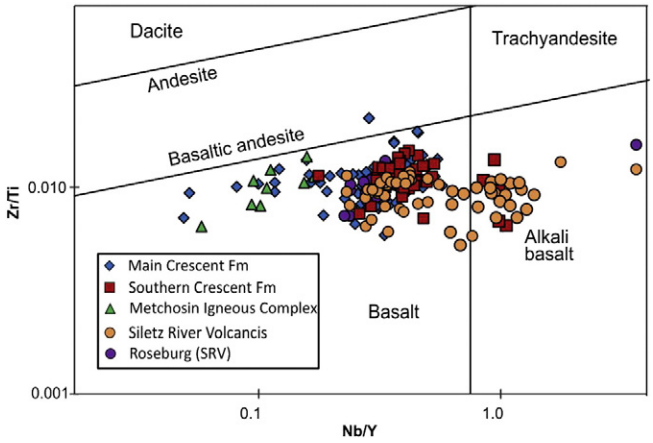

Fig. 3. Zr/Ti–Nb/Y classification diagram adapted from Pearce (1996).

as an enriched source or degree of partial melting. Other, more mobile, trace elements such as Sr display a positive correlation in most of the samples but much more scatter is evident. The Sm/Yb ratio varies from 0.35 to 5 for the main cluster of data, but extends up to 6.12 (Fig. 4). A similar pattern is apparent for the La/Yb ratio of the rocks, with a main cluster between 1 and 2 and extending up to ~33. In addition to this, a group of samples, mostly from the Metchosin Igneous Complex and the Crescent Formation, have lower (<1) Sm/Yb ratios.

On a primitive mantle normalised diagram (Fig. 5), samples from the Siletz River Volcanics and Crescent South and some samples from Roseburg show enrichment in the most incompatible elements relative to the less incompatible elements, while the remainder of samples show generally flat patterns. All samples show a large variation in Ba/Rb ratio, which is usually constant in unaltered oceanic basalts (Hofmann and White, 1983); this is consistent with Rb depletion during post-magmatic alteration. Chondrite-normalised REE patterns (Fig. 5) display flat to slightly depleted HREE and middle REE patterns (Dy/Yb ratio ranges between 1.5 and 3.4) (Fig. 6). The LREE in the Siletz samples show flat-to-enriched patterns, with several samples from the Siletz River Volcanics displaying the most enriched LREE patterns (La/Sm up to 9.8). There is little variation from east to west in the Dy/Yb ratio of the rocks of the Siletz terrane. The highest Dy/Yb values are found in the central part of the terrane (Fig. 6) and the lowest values are seen in the Metchosin Igneous Complex, the northernmost samples of the Crescent Terrane and from the Roseburg area in the southernmost part of the terrane. Some of these low Dy/Yb samples (from the Metchosin Igneous Complex) are also LREE depleted (Fig. 6).

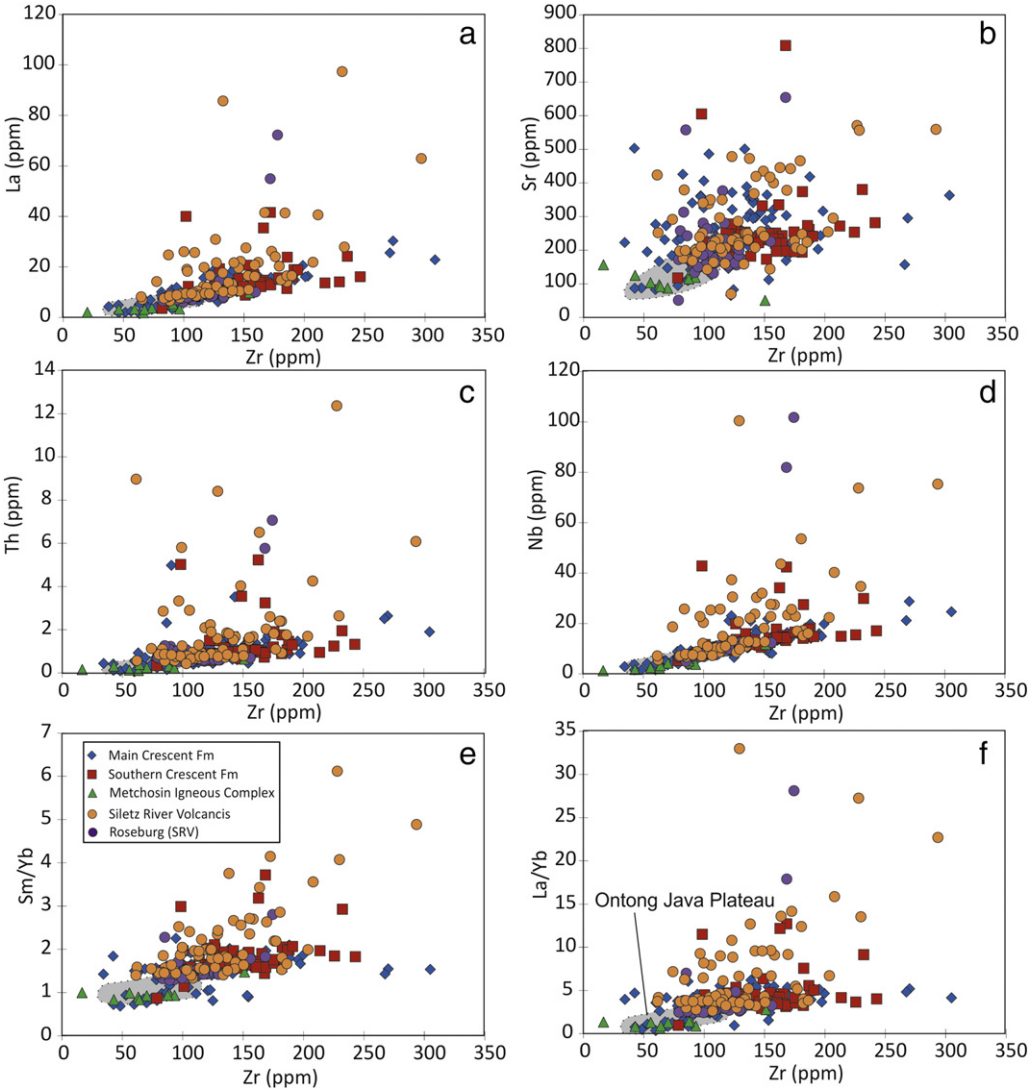

Fig. 4. Bivariate plots of trace element variations with Zr (ppm) for the Siletz terrane. Also shown in grey is the Ontong Java Plateau basalts compositional field (Fitton and Godard, 2004).

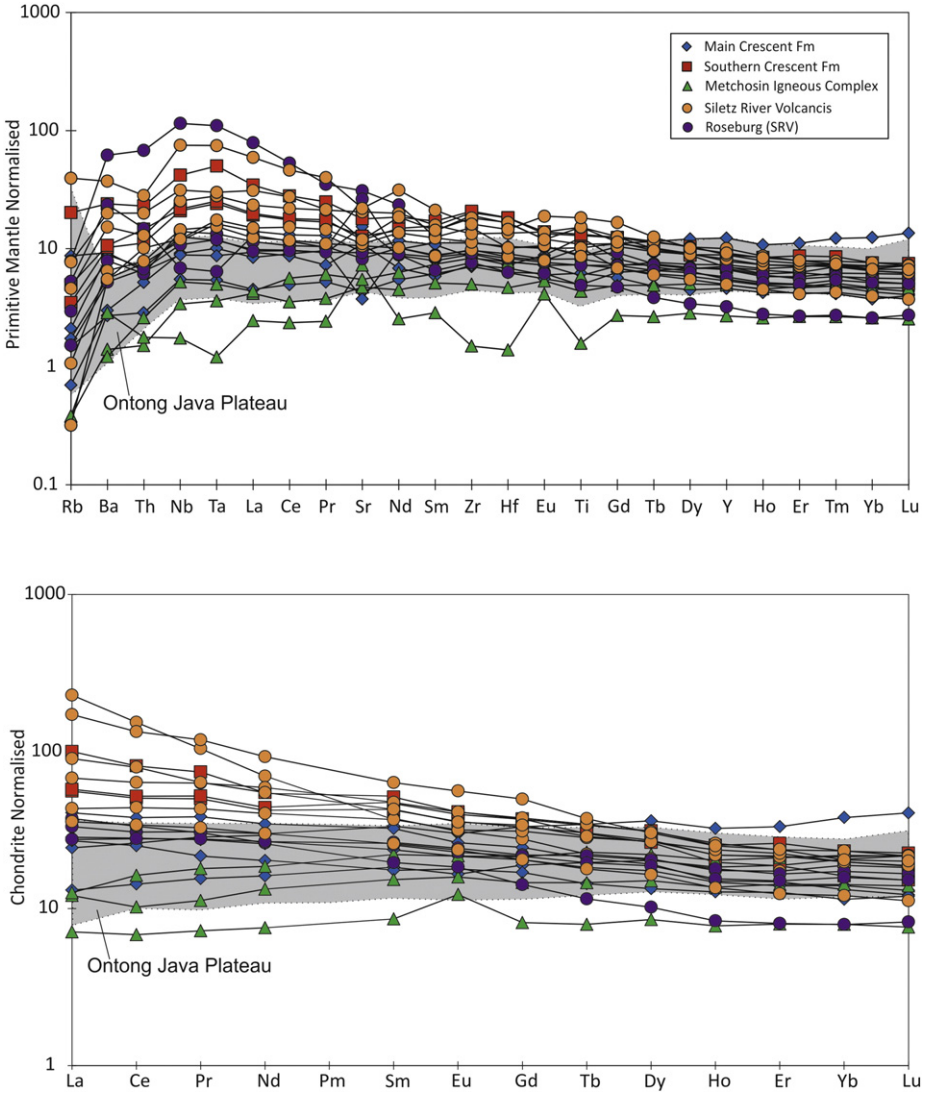

Fig. 5. Primitive mantle and chondrite-normalised trace element diagrams (normalising values from Sun and McDonough, 1989) of samples also analysed for isotopic ratios. For comparison the range of compositions of Ontong Java Plateau basalts is also shown (Fitton and Godard, 2004).

5.2. Sr-Nd-Hf-Pb radiogenic isotopes

The measured isotope ratios for the samples used in this study have been age corrected for in-situ decay between 54.5 and 50.5 Ma using the trace element abundances in Table 1 and Supplementary Material 4 and both the measured and initial values are reported in Table 2. The initial isotope ratios for the analysed samples range from $^{206}Pb/^{204}Pb$: 18.751 to 19.668, $^{207}Pb/^{204}Pb$: 15.507 to 15.661, $^{207}Pb/^{204}Pb$: 38.294 to 39.2128, $^{176}Hf/^{177}Hf$: 0.28300 to 0.28316 (ε_{Hf}: 9.0 to 14.5), $^{143}Nd/^{144}Nd$: 0.51282 to 0.51299 (ε_{Nd}: 5.0 to 8.1) and $^{87}Sr/^{86}Sr$: 0.70302 to 0.70380 (Table 2, Fig. 7) (ages used to correct the measured isotopic ratios are detailed in Supplementary Material 6). The Metchosin Igneous Complex samples display the most depleted and restricted isotope ratios of the entire Siletz terrane, and this is particularly evident in Hf–Nd isotopic space (Fig. 7d). The Crescent Formation samples show more variation in isotope ratios and this variation increases southward. The more-depleted Crescent Formation samples are still generally significantly more enriched than Pacific MORB compositions (Fig. 7). Samples CM230 and CM225 have elevated $^{87}Sr/^{86}Sr$ values compared to the other samples, which may be related to seawater alteration as all other isotope values for these samples are not anomalous. In particular Nd and Hf isotope systems are relatively resistant to alteration and so are likely to represent the primary composition of the rocks (White and Patchett, 1984; Nobre Silva et al., 2010).

The samples from northern Oregon and southern Washington (the Crescent South group of the Crescent formation, and the Siletz River Volcanics) show a similar amount of isotopic variation to one another, with the majority of samples from this area falling in the main cluster of data. The samples from the Roseburg area, in the south of the terrane, show the most isotopic variation. For example, Sample 073RB, which has the highest $^{206}Pb/^{204}Pb$ ratio of 19.668 and so plots closest to the HIMU mantle component in $^{206}Pb/^{204}Pb$ diagrams (Fig. 7), also has the highest La/Sm ratio of 9.8. Sample 095RB, also from the Roseburg area of the terrane, plots closest to EM2 and the Imnaha mantle component (IM) fields in all isotopic spaces (Fig. 7). The Imnaha component is thought to be the mantle plume source of the Columbia River Flood Basalts (CRFB) and the Snake–Yellowstone volcanics (Wolff et al., 2008).

There is little correlation between major and trace elements and isotope abundances with the exception of the more trace element-depleted samples (in comparison to the other more-enriched samples) (Fig. 5) also having the most depleted isotopic ratios of the terrane (Figs. 6 and 7). Samples with lower Pb and Sr isotopic ratios and higher ε_{Hf} and ε_{Nd} values also have the lowest La/Sm ratios (0.9–1.3) and the

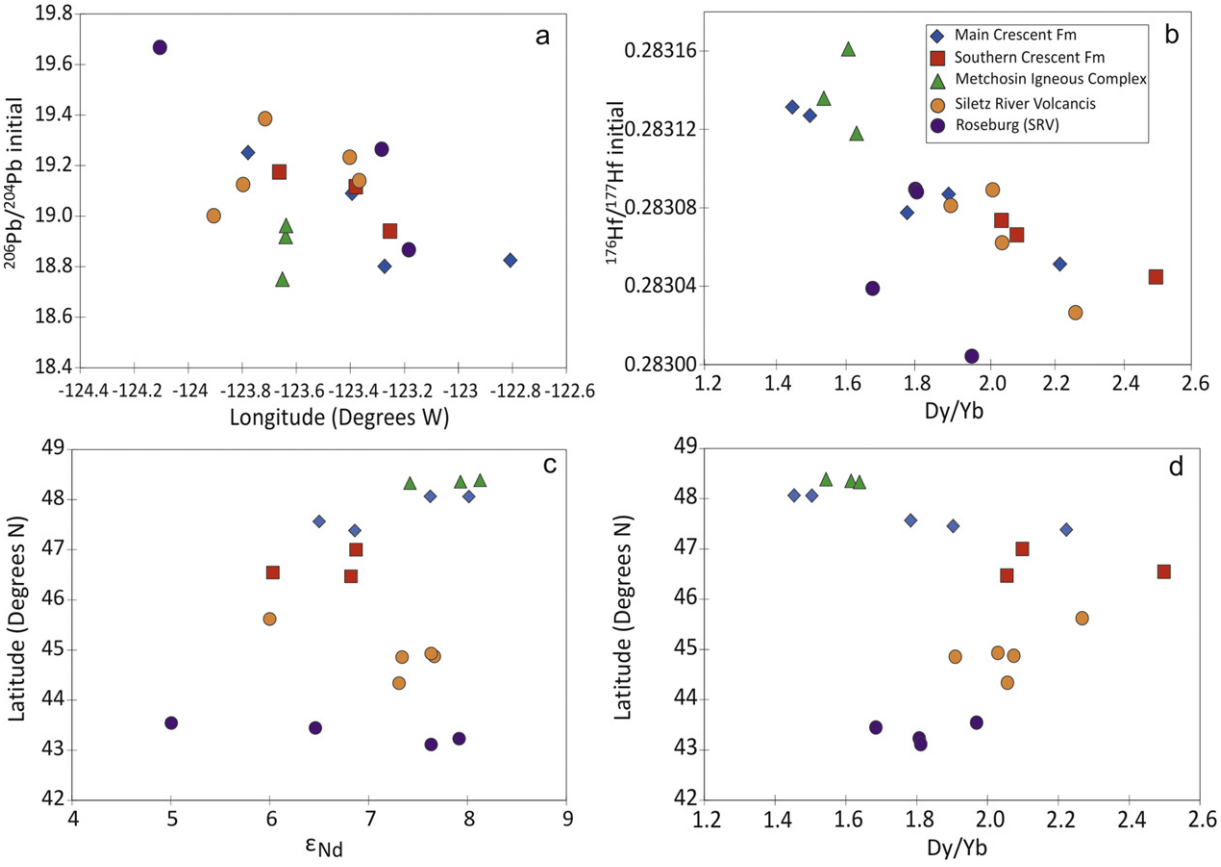

Fig. 6. a) $^{206}Pb/^{204}Pb$ (initial) vs. longitude, showing an overall decrease from West to East. b) $^{176}Hf/^{177}Hf$ (initial) vs. Dy/Yb which displays a noticeable inverse correlation. c) Latitude vs. εNd indicating an overall increase in variability southward across the terrane. d) Latitude vs. Dy/Yb ratio, showing little variation overall with the very lowest values corresponding to the northernmost part of the terrane.

most-depleted incompatible element abundances. There is also a negative correlation between Dy/Yb and Hf isotopic ratios (Fig. 6). As this trend is distinguishable in both trace elements and radiogenic isotopes it indicates that the differences observed are a reflection of the composition of the source regions rather than varying degrees of partial melting alone. The overall variation in isotopes generally increases southward across the terrane (Fig. 6).

All samples analysed have higher Pb isotopic ratios and $^{87}Sr/^{86}Sr$ values and lower $^{176}Hf/^{177}Hf$ and $^{143}Nd/^{144}Nd$ than the Pacific MORB Mantle (PMM) (Fig. 7). The Cobb Seamount chain (CS), a series of seamounts located near the East Pacific Rise (Chadwick et al., 2014), have consistently higher $^{143}Nd/^{144}Nd$ and lower $^{87}Sr/^{86}Sr$, $^{176}Hf/^{177}Hf$ and Pb isotopic ratios than the Siletz terrane samples. The Siletz terrane samples also generally overlap the Karmutsen Flood Basalt (KFB) field, which are a series of predominantly tholeiitic basalts located on Vancouver Island and form part of the accreted Jurassic aged Wrangellia oceanic plateau (Greene et al., 2009b) (Fig. 7). In Pb-Pb isotopic space the Siletz terrane shares similar isotopic characteristics to the Caribbean Plateau (Fig. 7).

6. Discussion

6.1. Mantle source composition

Although the samples analysed in this study span a range of compositions from basalts to more evolved rocks there is no correlation between the degree of fractionation undergone by each sample and the radiogenic isotope ratios. This indicates that the samples are unlikely to have been contaminated with lithospheric material during fractionation and are therefore likely to record the isotopic signature of the mantle source. Although no evidence for crustal contamination has been observed, some LREE enrichments are noted, which are most likely related to enriched components in the source or subsequent differentiation. In isotope plots (Fig. 7), the Siletz terrane data show similarity with the trends observed in the Karmutsen flood basalts, an oceanic plateau nearby and in a comparable setting (Greene et al., 2009b).

Binary mixing curves between MORB-source mantle and the Imnaha mantle component, EM2, and HIMU mantle components are shown in Fig. 7, with 10% increments. Trace element abundances used for the mantle components are discussed in Supplementary Material 7. A 53 Ma age corrected depleted Gorda MORB mantle (DGM) composition (Davis et al., 2008; Salters et al., 2011) was used as the end-member to represent a possible depleted mantle component.

The positive ε_{Hf} and ε_{Nd} values of all the Siletz samples reflect long-term incompatible element depletion of the source. In Pb-Pb, Pb-Nd and Pb-Hf isotopic space the Siletz data lie mostly between the DGM–HIMU and DGM–EM2 mixing curves (Fig. 7), while a dominance of EM2 is required in the other diagrams, especially in three samples, B019, 424CM and 095RB (and to a lesser extent 202MET). The Imnaha component also lies adjacent to the DGM-EM2 mixing curve, which indicates that the 3 samples with the significant EM2 component share similar isotopic signatures to the Columbia River Flood Basalts and the Snake River–Yellowstone hotspot trace (Wolff et al., 2008). Carlson (1984) also recognised that this component was present in the source of the CRFB, but proposed that it represented subducted sediment rather than a mantle plume component. However, the trace element data rule out the possibility of subducted sediment in the analysed samples as there is no 'arc signature' present in the mantle-normalised diagrams (i.e., no marked negative Nb-Ta anomaly or Th spike) (Fig. 5). Therefore, except for the 3 samples discussed above, the Siletz isotope data are

Table 2
Radiogenic isotope results.

Sample #	225CM	230CM	423CM	424CM	B019	450CS	374 CS	362 CS	392CS	205MET
$^{208}Pb/^{204}Pb$	38.7887		38.7246	38.6958	38.4750	38.7580	38.7620	39.1266	38.9244	38.7082
2SE	0.0029		0.0022	0.0047	0.0022	0.0023	0.0015	0.0019	0.0024	0.0020
$^{207}Pb/^{204}Pb$	15.5393		15.5493	15.5495	15.5224	15.5498	15.5541	15.5927	15.6247	15.5362
2SE	0.0011		0.0009	0.0016	0.0009	0.0009	0.0006	0.0008	0.0009	0.0009
$^{206}Pb/^{204}Pb$	19.2607		19.1790	19.1042	18.8581	19.1943	19.1743	19.4409	18.7681	19.0965
2SE	0.0013		0.0009	0.0023	0.0010	0.0011	0.0007	0.0009	0.0010	0.0011
$^{208}Pb/^{204}Pb$ i	38.781		38.691	38.332	38.431	38.724	38.737	39.085	38.821	38.626
$^{207}Pb/^{204}Pb$ i	15.539		15.545	15.533	15.521	15.548	15.553	15.591	15.620	15.533
$^{206}Pb/^{204}Pb$ i	19.252		19.089	18.763	18.823	19.163	19.151	19.403	18.678	19.028
$^{176}Hf/^{177}Hf$	0.283166	0.283175	0.283106	0.283070	0.283097	0.283079	0.283087	0.283054	0.282892	0.283196
2SE	0.000005	0.000006	0.000006	0.000005	0.000005	0.000006	0.000006	0.000007	0.000005	0.000007
$^{176}Hf/^{177}Hf$ i	0.28313	0.28313	0.28309	0.28306	0.28308	0.28306	0.28307	0.28304	0.28287	0.28317
ε_{Hf_i}	13.3	13.4	11.9	10.8	11.5	10.9	11.3	10.3	4.3	14.8
$^{143}Nd/^{144}Nd$	0.513058	0.513038		0.512985	0.512962	0.512990	0.512991	0.512943	0.512651	0.513055
2SE	0.000006	0.000005		0.000006	0.000007	0.000007	0.000008	0.000006	0.000008	0.000007
$^{143}Nd/^{144}Nd$ i	0.51298	0.51296		0.51292	0.51290	0.51293	0.51293	0.51289	0.51260	0.51297
ε_{Nd_i}	8.0	7.6		6.9	6.5	7.1	7.0	6.3	0.5	7.9
$^{87}Sr/^{86}Sr$		0.703813	0.703547	0.703137		0.703077	0.703086	0.703486	0.705287	0.703232
2SE		0.000009	0.000009	0.000008		0.000010	0.000009	0.000009	0.000007	0.000012
$^{87}Sr/^{86}Sr$ i		0.70380	0.70353	0.70300		0.70297	0.70307	0.70348		0.70316

quite different from that of the Imnaha component and require a difference source than the Columbia River Flood Basalts and Snake River–Yellowstone hotspot track.

There is a significant EM2 signature present in the majority of the data, indicating the presence of a deep mantle derived component (Weaver, 1991; Workman et al., 2004); this EM2 component is not as significant as in other Pacific OIBs, such as the Samoan Islands (Fig. 7). The most enriched samples display higher Dy/Yb values, indicating that these samples have undergone smaller amounts of melting of a deeper source relative to the more depleted samples (Fig. 6). The distinctive isotopic ratios of some of the samples may indicate that the lower melt fractions are preferentially sampling isotopically distinct enriched pods or plums (Cousens, 1996) or streaks within a mantle plume (Kerr et al., 1995).

As noted above the data also extend partially towards the HIMU component in Pb-Pb, Pb-Nd and Pb-Hf isotopic space (Fig. 7), indicating that this component may be present in the source of the Siletz basalts (especially in sample 073RB and to a lesser extent sample TK009). The involvement of a HIMU like signature is consistent with observations in other NE Pacific locations, such as the Cobb Seamounts (Chadwick et al., 2014), Explorer MORB (Cousens et al., in review), the Karmutsen flood basalt province (Greene et al., 2009a, 2009b) and the Garibaldi belt (Mullen and Weis, 2013). The samples which plot closest to HIMU have a more alkaline signature (highlighted in Fig. 7c) which suggests a relationship between the HIMU component and less extensive (deeper) melting, as is also observed at the Cobb Seamounts (Chadwick et al., 2014).

The PREMA component (Fig. 7) represents a common deep mantle component [or FOZO or C (Hanan and Graham, 1996; Stracke, 2012)]. It is also the Kea component in Hawaii and was interpreted to represent the average deep Pacific mantle (Nobre Silva et al., 2013). Some of the samples analysed from the Crescent Formation and Metchosin Igneous Complex lie adjacent to, or at the PREMA component composition in the Pb-Pb, Pb-Hf and Pb-Sr isotopic diagrams (Fig. 7c, d, e, f). However, while Siletz samples do appear to trend towards PREMA in some isotope diagrams (Pb-Pb), the majority of the Siletz terrane data, in most isotopic spaces, do not overlap with this component (Fig. 7). In addition, although it has been debated whether this signature actually exists as a discrete physical component, PREMA does appear to be a relatively common source composition for other well-characterised Pacific oceanic lavas, including the Hawaiian basalts (Fig. 7) (e.g., Nobre Silva et al., 2013), as well as those related to the Iceland and Yellowstone plumes (Hanan and Graham, 1996). Although the Siletz terrane isotopic data demonstrates some similarity to the trends observed in, for example, the Hawaiian Islands, most notably in Hf–Nd isotopic space, the Siletz terrane samples are distinctly more radiogenic in the Pb isotopic ratios together with lower $^{87}Sr/^{86}Sr$ (Fig. 7). Multiple components are therefore most likely required to explain the trends observed in the isotopic data (Fig. 7) i.e., a depleted component isotopically similar to DGM, along with an enriched signature that straddles between EM2 and HIMU. The enriched signature, although prevalent throughout the terrane, is less apparent in the samples from the north-east, i.e., the Metchosin Igneous Complex and some Crescent Formation samples (Fig. 7).

6.2. Mantle source T and P conditions

We have also attempted to determine the pressure and temperature of the mantle source region of the basalts of the Siletz terrane (Supplementary Material 8). Due to the relatively low magnesium contents and abundant clinopyroxene fractionation, few of the samples are suitable for the calculations. The methods outlined in Lee et al. (2009), which are based on Si and Mg contents of the magma resulted in only 7 samples producing mantle temperature and pressures, while the PRIMELTS 3 modelling software of Herzberg and Asimow (2015) produced results for 30 samples, 7 of which are in agreement with the temperature and pressure values obtained using the modelling of Lee et al. (2009). The results for these 7 samples were relatively consistent across the two techniques, producing a range of initial mantle potential temperatures (Tp) between ~1400 and 1500 °C and pressures between 1.5 GPa and 2.4 GPa (i.e., melting at less than 100 km). Mid-ocean ridge basalts display Tp ranges between ~1280 and 1400 °C, while intra-plate magmas are produced at Tp above >1400 °C (Herzberg et al., 2007; Lee et al., 2009). The Tp conditions estimated for the Siletz terrane data therefore support a mantle plume related origin for the Siletz terrane. The PRIMELTS 3 modelling results also require an olivine addition of on average 39% which indicates that subsequent to melting of the source, the magma is likely to have undergone significant fractionation in a crustal magma chamber to generate the observed compositions.

The results of this modelling, in combination with the isotopic data discussed in the previous section, indicate that the melts forming the Siletz terrane were derived from a heterogeneous and partially enriched

207MET	202MET	073RB	042 RB	095 RB	068RB	116SRV	144SRV	150SRV	CR011	TK009
38.5715	38.3307	39.4752	38.7880	38.5914		38.9278	38.6587	38.6768	38.9113	39.1397
0.0018	0.0019	0.0031	0.0030	0.0023		0.0025	0.0028	0.0030	0.0030	0.0025
15.5273	15.5091	15.6173	15.5510	15.5918		15.5641	15.5516	15.5356	15.5650	15.5974
0.0007	0.0007	0.0009	0.0012	0.0007		0.0010	0.0009	0.0011	0.0010	0.0008
18.9909	18.7884	19.8567	19.2733	18.9291		19.4013	19.0478	19.1604	19.3876	19.4326
0.0008	0.0007	0.0011	0.0013	0.0009		0.0010	0.0011	0.0013	0.0015	0.0011
38.551	38.294	39.220	38.781	38.532		38.912	38.615	38.658	38.592	38.984
15.527	15.507	15.609	15.551	15.589		15.563	15.549	15.535	15.552	15.588
18.975	18.750	19.673	19.265	18.869		19.385	19.001	19.140	19.120	19.224
0.283182	0.283168	0.283060	0.283111	0.283020	0.283110		0.283106	0.283107	0.283075	0.283042
0.000004	0.000005	0.000005	0.000005	0.000006	0.000005		0.000006	0.000008	0.000004	0.000004
0.28315	0.28315	0.28304	0.28309	0.28301	0.28308		0.28308	0.28309	0.28306	0.28303
14.2	14.0	10.2	12.0	9.0	11.6		11.7	11.9	9.7	11.0
0.513028	0.513067	0.512937	0.513035	0.512877	0.513025	0.513022	0.513008	0.513016	0.512998	0.512925
0.000005	0.000007	0.000007	0.000005	0.000006	0.000008	0.000004	0.000006	0.000008	0.000007	0.000008
0.51295	0.51299	0.51290	0.51298	0.51283	0.51296	0.51296	0.51295	0.51296	0.51294	0.51288
7.5	8.1	6.4	7.9	5.0	7.6	7.7	7.3	7.6	7.3	6.0
0.703285	0.703407	0.703294	0.703126	0.703553		0.703056	0.703136	0.703057	0.703061	0.703395
0.000010	0.000010	0.000009	0.000009	0.000007		0.000008	0.000008	0.000007	0.000010	0.000009
0.70323		0.70328	0.70310	0.70354		0.70305	0.70313	0.70304	0.70304	0.70311

mantle source, with an elevated temperature. The volume of melt produced (~2.6×10^6 km^3; Trehu et al., (1994)) is consistent with extensive melting in a mantle plume head (Fitton and Godard, 2004; Herzberg and Gazel, 2009). While the range in calculated pressures may indicate inaccuracies in the models they may also point to melting over a significant range of depths which may represent the interaction of a plume and depleted mantle (Fig. 7). The amount of melting modelled in PRIMELTS3 is also indicative of a hotter-than-ambient mantle source with melting percentages of ~27% (with the majority of samples producing results between 25 and 33%), which are comparable to the extent of melting calculated for the Ontong Java Plateau and the Caribbean Plateau (~30% melting) (Fitton and Godard, 2004; Herzberg and Gazel, 2009).

6.3. Tectonic implications

There have been many tectonic models proposed to explain the origin of the Siletz terrane and its resulting geochemical and physical characteristics. One model which may explain the characteristics of the Siletz terrane is its formation in a marginal basin setting (Brandon, 2014; Wells et al., 1984), yet this does not accurately explain the proposed geometry of the plates at the time of eruption (Wells et al., 2014), the enriched isotopic signatures, nor the lack of arc signatures in the Siletz terrane (Fig. 5).

Another suggested model of formation for the Siletz terrane proposes subduction initiation along a transform fault, which can explain both the linear geometry of the terrane and its suggested volume (Stern, 2004). In this model a transform fault parallel to the North American margin between the Farallon and the partially subducted Kula/Resurrection plate represents a zone of weakness along which subduction can propagate (Babcock et al., 1992; Denny, 2012; Haeussler et al., 2003; Stern, 2004; Wells et al., 1998). The composition of the Siletz basalts does not support an early-arc tectonic setting resulting from subduction initiation as the primary mechanism of formation of the Siletz terrane. Isotopically, the Siletz basalts are much more enriched than those related to subduction initiation, e.g., in the basalts of the Izu Bonin and Mariana areas (Arculus et al., 2015; Stern, 2004).

An alternative model proposed is the slab window model (Babcock et al., 1992). This model is not supported by the initial temperatures calculated for the mantle source of the Siletz terrane, as the temperature of primary magmas derived from slab windows are thought to be comparable to mid-ocean ridges (1300–1400 °C) (Hastie and Kerr, 2010), compared to 1400–1500 °C calculated for the Siletz terrane. The suggested characteristics of the mantle source of the Siletz terrane are also more enriched than the DMM-like mantle that is thought to produce slab window related magmatism (Hastie and Kerr, 2010; Herzberg et al., 2007). Finally, the trace elements of Siletz rocks do not generally display typical subduction-related characteristics, such as Nb-Ta depletions or Th enrichments (Figs. 3 and 4) (Pearce, 2008).

The lack of uniform resemblance to the Imnaha component in the majority of Siletz samples appears to rule out the Yellowstone hotspot mantle plume head as a source region (Pyle et al., 2009). However, the composition of the plume source is unlikely to have been consistent over time, or may be heterogeneous, and therefore variation in the amount of melting for example may result in the sampling of parts of the plume with markedly different compositions (Escuder-Viruete et al., 2007; Kerr et al., 1995). In addition to this, several plate reconstructions propose that the Yellowstone hotspot was present in this area at the time of the formation of the Siletz terrane (Doubrovine et al., 2012; Müller et al., 1993; O'Neill et al., 2005).

Volcanic ash layers/tuffs are typically unusual in oceanic plateaus (Kerr, 2014), while there are abundant volcanoclastic horizons throughout the terrane, especially in the upper subaerial flows. Progressive shallowing throughout the sequence from deep to shallow water to subaerial environments indicates continual dynamic uplift by the plume (as well as accumulation of the lava pile) while also explaining the abundance of ash and volcanoclastic material. This has also been observed at other well-characterised mantle plume-related oceanic plateaus, such as in the Western Cordillera of Colombia, in the Caribbean Plateau (Kerr, 2014) and also in limited occurrences in the Ontong Java Plateau where tuff layers and sedimentary reworking occur (Mahoney et al., 2001).

The Siletz basalts are most depleted in the north and northeast, becoming more enriched in the central and southern areas and towards the west. The basalts are represented by a range of moderately enriched compositions (E-MORB-like) with even the most depleted samples being more enriched than typical N-MORB. The depth of melting also appears to increase towards the centre of the terrane. Sample 073RB is the most western sample and additionally has the largest HIMU component.

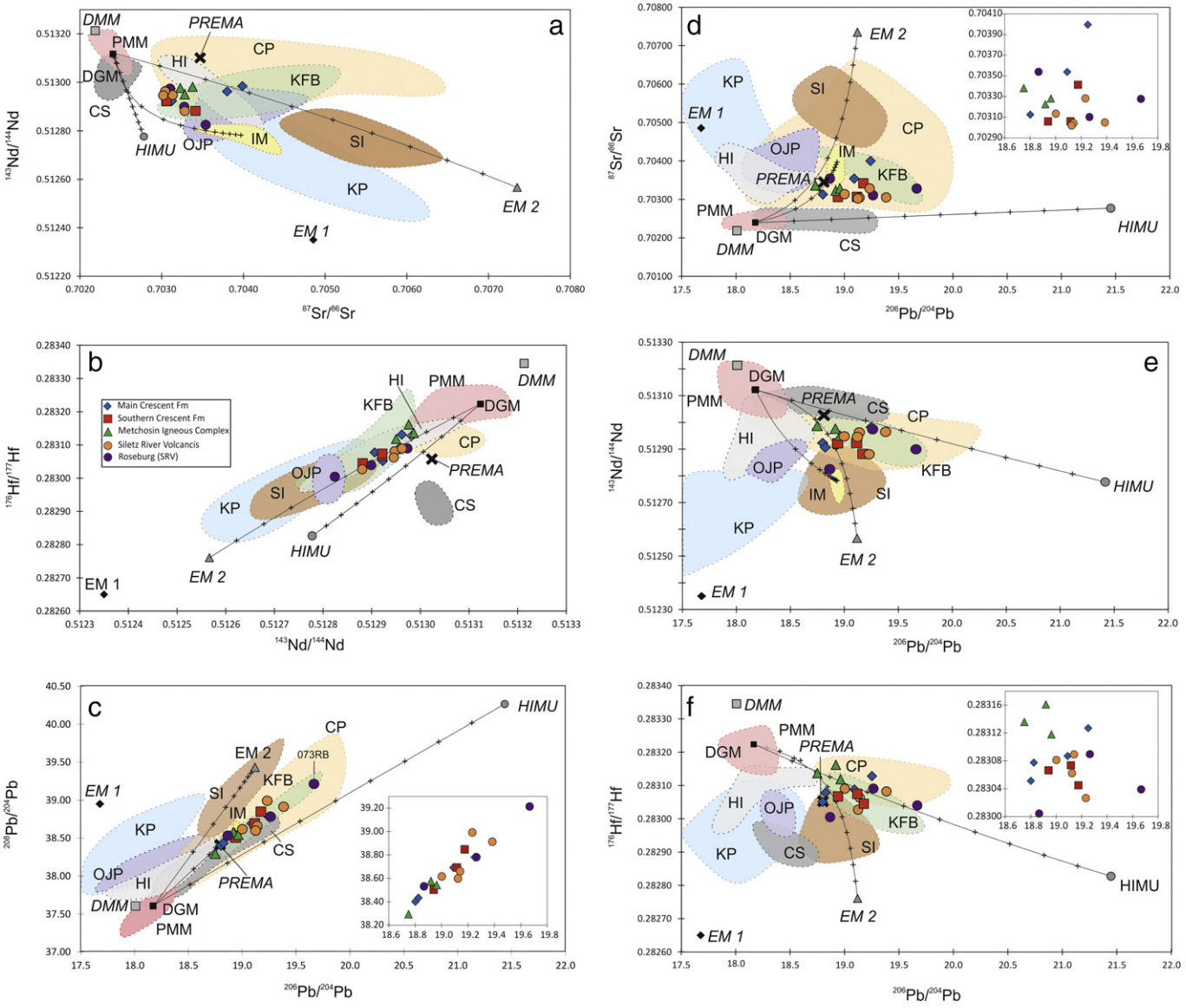

Fig. 7. Initial isotope ratios of the Siletz terrane samples. Also plotted are age-corrected (53 Ma) isotope ratios for mantle components (Supplementary Material 7), PMM - Pacific MORB mantle (Chauvel and Blichert-Toft, 2001), DGM - Depleted Gorda MORB mantle (Davis et al., 2008; Salters et al., 2011), IM - Imnaha mantle component (source of the primary Columbia River Flood basalts and thought to represent the Yellowstone hotspot; (Wolff et al., 2008)), CS - Cobb seamount chain (a series of seamounts located near the East Pacific Rise; (Chadwick et al., 2014)), and KFB - Karmutsen flood basalts of the Wrangellia terrane, Vancouver Island (Greene et al., 2009b). Also shown are compositional fields of the Ontong Java Plateau (OJP) (Mahoney et al., 1993a, 1993b; Tejada et al., 2002, 2004), Caribbean Plateau (CP) (Hastie et al., 2008; Hauff et al., 2000; Kerr et al., 1997, 2002b; Thompson et al., 2004), Kerguelen Plateau (KP) (Weis and Frey, 2002; Weis et al., 2002), the Hawaiian Islands (HI) (Garcia et al., 2010; Tanaka et al., 2002; Weis et al., 2011) and the Samoan Islands (SI) (Salters et al., 2011; Workman et al., 2004). Error bars for the Siletz terrane data are smaller than the symbols. Binary mixing curves between DGM and the Imnaha mantle component, EM2 and HIMU mantle components are also shown, where each increment represents 10% addition of the mixing component to the DGM.

Overall, the mantle characteristics of the Siletz terrane best represent mixing of depleted mantle with an additional enriched input from a mantle plume. The temperature of the primary magmas has been calculated at 1400–1500 °C, which is hotter than ambient mid-ocean-ridge related mantle. The enriched component and mantle plume source has been proposed to represent the Yellowstone hotspot (Fig. 8) (cf. Duncan, 1982; McCrory and Wilson, 2013; Wells et al., 2014). The depleted mantle source component recorded in the relatively depleted samples from the NE (the Metchosin Igneous Complex and Crescent Formation) is comparable to mid-ocean ridge source mantle (more extensive melting), most likely the Farallon–Kula/Resurrection ridge, and the off axis interaction of an additional hotter enriched mantle source region (Fig. 8). Alternatively, the depleted component may be sampling a depleted relatively refractory portion of the mantle plume (Kempton et al., 2000; Kerr et al., 1995).

6.4. Youngest oceanic plateau?

Oceanic plateaus represent vast areas of over-thickened predominantly basaltic oceanic crust (>5 × 10^5 km^3) the majority of which erupted over a few million years (Kerr, 2014). Elevated topography and greater crustal thickness in comparison with 'normal' oceanic crust lead to an increase in buoyancy in oceanic plateaus. Therefore, notably for plateaus that collide with subduction zones shortly after formation (<5 Ma), the probability of partial accretion to the adjacent upper continental plate margin and so preservation within the geologic record is greatly increased (Cloos, 1993). Accreted oceanic plateaus

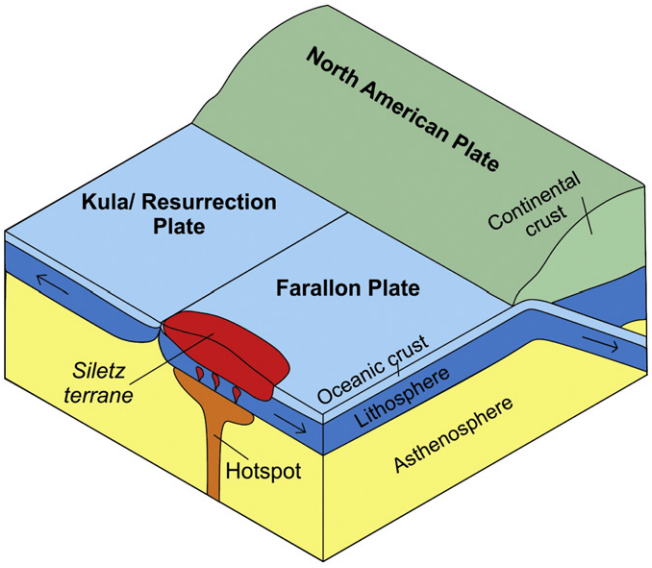

Fig. 8. Schematic diagram of the tectonic setting in which the rocks of the Siletz terrane were formed.

have had a significant role in the growth of the continental crust; however, secondary processes such as deformation and burial lead to difficulties in the recognition of their characteristics once accreted (Kerr et al., 2000). Despite this, many examples of crustal growth through oceanic plateau accretion have been recognised in the geological record, including sections of the Wrangellia terrane (Greene et al., 2009a, 2009b), which along with the Siletz terrane highlights the role of oceanic plateaus in the growth and evolution of the western margin of North America.

Several well-characterised oceanic plateaus have similar heterogeneous trace element compositions to the Siletz terrane, e.g., the Cretaceous Caribbean plateau (Kerr and Mahoney, 2007) and the Late Triassic (ca. 225–231 Ma) Karmusten flood basalts of Vancouver Island and Alaska (Greene et al., 2009a, 2009b). In contrast, the largest oceanic plateau, the Cretaceous Ontong Java Plateau, is more depleted and anomalously homogeneous in composition (Fitton and Godard, 2004) (Figs. 4 and 6). While geochemistry alone cannot be used to distinguish oceanic plateaus in the geological record, their Nb/La ratio is often ~1 (Kerr, 2014), and this is generally reflected in the Siletz terrane data, which clusters between ratios of 1 and 1.5. Samples also show similar flat-to-LREE-enriched patterns with no significant Nb-Ta depletions or Th enrichments (Fig. 5).

Features of the terrane which support an oceanic plateau origin include; moderately enriched isotopic compositions, flat to slightly enriched REE patterns and the vast size and magmatic volume of the terrane (estimated to be 2.6×10^6 km^3; Trehu et al., 1994), the bulk of which erupted within 5–7 Ma. In addition to this, mantle melt modelling for the Siletz terrane (as discussed above) indicates elevated mantle source potential temperatures, and similar amounts of partial melting and subsequent fractionation to the Caribbean and Ontong Java Plateaus. The terrane does, however, thin to 10 km at Vancouver Island and 6 km offshore, which is more typical of normal oceanic crust, compared to the average ~20 km thickness estimated for the remainder of the terrane (Hyndman et al., 1990; Parsons et al., 1999; Trehu et al., 1994). Sheeted dykes present at Bremerton (Crescent Formation) and on Vancouver Island (Metchosin Igneous Complex), which while unusual in other oceanic plateaus (Kerr, 2014), are consistent with plume–ridge interaction. Finally, as discussed above, there are relatively depleted signatures present in some sequences from the north of the terrane, comparable to mid-oceanic ridge environments. Overall, the accumulated evidence appears to support the conclusion that the Siletz terrane is an accreted oceanic plateau, and hence represents the youngest oceanic plateau thus far characterised.

7. Conclusions

1. The Siletz accreted mafic terrane has a large magmatic volume (2.6×10^6 km^3) (Trehu et al., 1994) which represents a sequence of rocks that progressively shallow from marine to terrestrial environments and erupted over a relatively short time period (56–49 Ma).
2. The rocks of the terrane are geochemically comparable, both in trace element (generally flat to LREE enriched REE patterns) and radiogenic isotope composition, to several well characterised oceanic plateaus.
3. The estimated initial mantle potential temperatures of 1400–1500 °C and the amount of partial melting undergone, ~ 25–33%, is similar to other mantle plume derived provinces such as the Ontong Java Plateau and the Caribbean plateau (Fitton and Godard, 2004; Herzberg and Gazel, 2009).
4. The mafic rocks of the Siletz terrane appear to have been derived from a heterogeneous and partially enriched mantle source with an above ambient temperature. This source composition is comprised of a relatively depleted signature and EM2- and HIMU-like enrichments. The enriched components may therefore represent melting of a heterogeneous mantle plume, possibly the Yellowstone Hotspot, which likely interacted with a mid-oceanic ridge, the Kula–Farallon (or Farallon–Resurrection) ridge.
5. Although individually, the geochemical signatures and physical characteristics of the Siletz terrane can be interpreted differently, when taken together, the evidence for the Siletz terrane representing an accreted oceanic plateau linked to a mantle plume is compelling.

Acknowledgements

The research presented in this paper forms part of a PhD dissertation undertaken by B.A. Phillips at Cardiff University. Iain McDonald is thanked for the major and trace element analyses of the samples. We thank Bruno Kieffer for the TIMS analyses and Kathy Gordon and Liyan Xing for assistance with MC-ICP-MS analyses. We thank John Wolff and an anonymous reviewer for their comments which helped clarify our scientific arguments. This work was supported by a Natural Environmental Research Council doctoral training grant (grant number NE/L501773/1) and NSERC Discovery Grant to D. Weis.

Appendix A. Supplementary data

Supplementary data to this article can be found online at http://dx.doi.org/10.1016/j.lithos.2017.01.005.

References

Arculus, R.J., Ishizuka, O., Bogus, K.A., Gurnis, M., Hickey-Vargas, R., Aljahdali, M.H., Bandini-Maeder, A.N., Barth, A.P., Brandl, P.A., Drab, L., 2015. A record of spontaneous subduction initiation in the Izu-Bonin-Mariana arc. Nature Geoscience 8, 728–733.

Atwater, T., 1989. Plate Tectonic History of the Northeast Pacific and Western North America: the Eastern Pacific Ocean and Hawaii: Boulder, Colorado. Geological Society of America, Geology of North America N, pp. 21–72 (ISBN: 0813752086).

Babcock, R.S., Burmester, R.F., Engebretson, D.C., Warnock, A., Clark, K.P., 1992. A rifted margin origin for the crescent basalts and related rocks in the Northern Coast Range Volcanic Province, Washington and British-Columbia. Journal of Geophysical Research - Solid Earth 97:6799–6821. http://dx.doi.org/10.1029/91jb02926.

Brandon, M.T., 2014. New evidence for backarc basin interpretation for Eocene coast-range terrane. Proceedings 2014 GSA Annual Meeting in Vancouver, British Columbia 2014.

Breitsprecher, K., Thorkelson, D., Groome, W., Dostal, J., 2003. Geochemical confirmation of the Kula-Farallon slab window beneath the Pacific Northwest in Eocene time. Geology 31, 351–354.

Cady, W., 1975. Tectonic setting of the Tertiary volcanic rocks of the Olympic Peninsula, Washington. Journal of Research of the US Geological Survey 3, 573–582.

Cann, J.R., 1970. Rb, Sr, Y, Zr and Nb in some ocean floor basaltic rocks. Earth and Planetary Science Letters 10, 7–11.

Carlson, R.W., 1984. Isotopic constraints on Columbia River flood basalt genesis and the nature of the subcontinental mantle. Geochimica et Cosmochimica Acta 48 (11), 2357–2372.
Chadwick, J., Keller, R., Kamenov, G., Yogodzinski, G., Lupton, J., 2014. The Cobb hot spot: HIMU-DMM mixing and melting controlled by a progressively thinning lithospheric lid. Geochemistry, Geophysics, Geosystems 15:3107–3122. http://dx.doi.org/10.1002/2014GC005334.
Chauvel, C., Blichert-Toft, J., 2001. A hafnium isotope and trace element perspective on melting of the depleted mantle. Earth and Planetary Science Letters 190, 137–151.
Chen, L., Sun, Y., Pei, X., Gao, M., Feng, T., Zhang, Z., Chen, W., 2001. Northernmost paleo-tethyan oceanic basin in Tibet: geochronological evidence from $^{40}Ar/^{39}Ar$ age dating of Dur'ngoi ophiolite. Chinese Science Bulletin 46 (14), 1203–1205.
Cloos, M., 1993. Lithospheric buoyancy and collisional orogenesis: subduction of oceanic plateaus, continental margins, island arcs, spreading ridges, and seamounts. Geological Society of America Bulletin 105, 715–737.
Condie, K.C., 1998. Episodic continental growth and supercontinents: a mantle avalanche connection? Earth and Planetary Science Letters 163, 97–108.
Cousens, B.L., 1996. Depleted and enriched upper mantle sources for basaltic rocks from diverse tectonic environments in the northeast Pacific Ocean: the generation of oceanic alkaline vs. tholeiitic basalts. In: Basu, A., Hart, S. (Eds.), Earth Processes: Reading the Isotopic Code. American Geophysical Union, Washington, D. C.:pp. 20–231 http://dx.doi.org/10.1029/GM095p0207.
Cousens, B., Weis, D., Constantin, M., Scott, S., 2016. Radiogenic isotopes in enriched mid-ocean ridge basalts from Explorer Ridge, Northeast Pacific Ocean: The HIMU Connection. Geochimica et Cosmochimica Acta (in review).
Davis, A.S., Plafker, G., 1986. Eocene basalts from the Yakutat terrane: evidence for the origin of an accreting terrane in southern Alaska. Geology 14, 963–966.
Davis, A., Clague, D., Cousens, B., Keaten, R., Paduan, J., 2008. Geochemistry of basalt from the north Gorda segment of the Gorda ridge: evolution toward ultraslow spreading ridge lavas due to decreasing magma supply. Geochemistry, Geophysics, Geosystems 9. http://dx.doi.org/10.1029/2007GC001775.
Denny, A.C., 2012. Geochemistry of the Lower Crescent Formation, Washington, and Re-evaluation of Proposed Formation Hypotheses. Carleton College, Northfield, Minnesota.
Doubrovine, P.V., Steinberger, B., Torsvik, T.H., 2012. Absolute plate motions in a reference frame defined by moving hot spots in the Pacific, Atlantic, and Indian oceans. Journal of Geophysical Research - Solid Earth 117 (B9), 2156–2202.
Duncan, R.A., 1982. A captured island chain in the Coast Range of Oregon and Washington. Journal of Geophysical Research 87 (NB13), 827–837.
Engebretson, D.C., 1985. Relative Motions between Oceanic and Continental Plates in the Pacific Basin. Geological Society of America 1–60.
Escuder-Viruete, J., Perez-Estaun, A., Contreras, F., Joubert, M., Weis, D., Ullrich, T.D., Spadea, P., 2007. Plume mantle source heterogeneity through time: insights from the Duarte Complex, Hispaniola, northeastern Caribbean. Journal of Geophysical Research - Solid Earth 112, B4.
Fitton, J.G., Godard, M., 2004. Origin and evolution of magmas on the Ontong Java Plateau. In: Fitton, J.G., Mahoney, J.J., Wallace, P.J., Saunders, A.D. (Eds.), Origin and Evolution of the Ontong Java Plateau. Geological Society of London, Special Publication vol. 229, pp. 151–178.
Fleming, S.W., Trehu, A.M., 1999. Crustal structure beneath the central Oregon convergent margin from potential-field modeling: evidence for a buried basement ridge in local contact with a seaward dipping backstop. Journal of Geophysical Research - Solid Earth 104 (B9), 20431–20447.
Gao, H., Humphreys, E.D., Yao, H., van der Hilst, R.D., 2011. Crust and lithosphere structure of the northwestern US with ambient noise tomography: terrane accretion and cascade arc development. Earth and Planetary Science Letters 304, 202–211.
Garcia, M.O., Swinnard, L., Weis, D., Greene, A.R., Tagami, T., Sano, H., Gandy, C.E., 2010. Petrology, geochemistry and geochronology of Kaua'i lavas over 4–5 Myr: implications for the origin of rejuvenated volcanism and the evolution of the Hawaiian plume. Journal of Petrology 51(7), 1507–1540.
Greene, A.R., Scoates, J.S., Weis, D., Israel, S., 2009a. Geochemistry of Triassic flood basalts from the Yukon (Canada) segment of the accreted Wrangellia oceanic plateau. Lithos 110, 1–19.
Greene, A.R., Scoates, J.S., Weis, D., Nixon, G.T., Kieffer, B., 2009b. Melting history and magmatic evolution of basalts and picrites from the accreted Wrangellia oceanic plateau, Vancouver Island, Canada. Journal of Petrology 50, 467–505.
Groome, W.G., Thorkelson, D.J., Friedman, R.M., Mortensen, J.K., Massey, N.W., Marshall, D.D., Layer, P.W., 2003. Magmatic and Tectonic History of the Leech River Complex, Vancouver Island, British Columbia: Evidence for Ridge-Trench Intersection and Accretion of the Crescent Terrane. Special Papers - Geological Society of America pp. 327–354.
Haeussler, P., Clark, J., Kenneth, P., 2000. Geologic Map of the Wildcat Lake 7.5'Quadrangle Kitsap and Mason Counties, Washington. Geological Survey Open-File Report 00-356.
Haeussler, P.J., Bradley, D.C., Wells, R.E., Miller, M.L., 2003. Life and death of the resurrection plate: evidence for its existence and subduction in the northeastern Pacific in Paleocene-Eocene time. Geological Society of America Bulletin 115, 867–880.
Hanan, B.B., Graham, D.W., 1996. Lead and helium isotope evidence from oceanic basalts for a common deep source of mantle plumes. Science 272 (5264), 991–995.
Hastie, A.R., Kerr, A.C., 2010. Mantle plume or slab window?: physical and geochemical constraints on the origin of the Caribbean oceanic plateau. Earth-Science Reviews 98 (3–4):283–293. http://dx.doi.org/10.1016/j.earscirev.2009.11.001.
Hastie, A.R., Kerr, A.C., Pearce, J.A., Mitchell, S., 2007. Classification of altered volcanic island arc rocks using immobile trace elements: development of the Th–Co discrimination diagram. Journal of Petrology 48 (12), 2341–2357.
Hastie, A.R., Kerr, A.C., Mitchell, S.F., Millar, I.L., 2008. Geochemistry and petrogenesis of Cretaceous oceanic plateau lavas in eastern Jamaica. Lithos 101 (3–4), 323–343.
Hauff, F., Hoernle, K., van den Bogaard, P., Alvarado, G.E., Garbe-Schonberg, C.D., 2000. Age and geochemistry of basaltic complexes in western Costa Rica: contributions to the geotectonic evolution of Central America. Geochemistry, Geophysics, Geosystems 1. http://dx.doi.org/10.1029/1999GC000020.
Herzberg, C., Asimow, P., 2015. PRIMELT3 MEGA. XLSM software for primary magma calculation: peridotite primary magma MgO contents from the liquidus to the solidus. Geochemistry, Geophysics, Geosystems 16 (2):563–578. http://dx.doi.org/10.1002/2014GC005631.
Herzberg, C., Gazel, E., 2009. Petrological evidence for secular cooling in mantle plumes. Nature 458, 619–622.
Herzberg, C., Asimow, P.D., Arndt, N., Niu, Y., Lesher, C.M., Fitton, J.G., Cheadle, M.J., Saunders, A.D., 2007. Temperatures in ambient mantle and plumes: constraints from basalts, picrites, and komatiites. Geochemistry, Geophysics, Geosystems 8. http://dx.doi.org/10.1029/2006GC001390.
Hirsch, D.M., Babcock, R.S., 2009. Spatially heterogeneous burial and high-P/T metamorphism in the Crescent Formation, Olympic Peninsula, Washington. American Mineralogist 94 (8–9), 1103–1110.
Hofmann, A.W., White, W.M., 1983. Ba, Rb and Cs in the Earth's mantle. Zeitschrift für Naturforschung 38a, 256–266.
Hyndman, R., Yorath, C., Clowes, R., Davis, E., 1990. The northern Cascadia subduction zone at Vancouver Island: seismic structure and tectonic history. Canadian Journal of Earth Sciences 27 (3), 313–329.
Ichiyama, Y., Ishiwatari, A., Kimura, J.-I., Senda, R., Miyamoto, T., 2014. Jurassic plume-origin ophiolites in Japan: accreted fragments of oceanic plateaus. Contributions to Mineralogy and Petrology 168 (1), 1–24.
Irving, E., 1979. Paleopoles and paleolatitudes of North America and speculations about displaced terrains. Canadian Journal of Earth Sciences 16 (3), 669–694.
Kempton, P.D., Fitton, J.G., Saunders, A.D., Nowell, G.M., Taylor, R.N., Hardarson, B.S., Pearson, G., 2000. The Iceland plume in space and time: a Sr-Nd-Pb-Hf study of the North Atlantic rifted margin. Earth and Planetary Science Letters 177 (3–4), 255–271.
Kerr, A.C., 2014. Oceanic plateaus. In: Holland, H.C., Turekian, K. (Eds.), Treatise on Geochemistry, 2nd Edition. Volume 4 Rudnick, R. (Ed.) The Crust. Chapter 18, 631-667. Elsevier. ISBN: 9780080983004.
Kerr, A.C., Mahoney, J.J., 2007. Oceanic plateaus: problematic plumes, potential paradigms. Chemical Geology 241 (3–4), 332–353.
Kerr, A.C., Saunders, A.D., Tarney, J., Berry, N.H., Hards, V.L., 1995. Depleted mantle plume geochemical signatures: no paradox for plume theories. Geology 23, 843–846.
Kerr, A., Marriner, G., Tarney, J., Nivia, A., Saunders, A., Thirlwall, M., Sinton, C., 1997. Cretaceous Basaltic Terranes in western Columbia: elemental, chronological and Sr–Nd isotopic constraints on petrogenesis. Journal of Petrology 38 (6), 677–702.
Kerr, A.C., White, R.V., Saunders, A., 2000. LIP reading: Recognizing oceanic plateaux in the geological record. Journal of Petrology 41, 1041–1056.
Kerr, A.C., Aspden, J.A., Tarney, J., Pilatasig, L.F., 2002a. The nature and provenance of accreted oceanic terranes in western Ecuador: geochemical and tectonic constraints. Journal of the Geological Society 159, 577–594.
Kerr, A.C., Tarney, J., Kempton, P.D., Spadea, P., Nivia, A., Marriner, G.F., Duncan, R.A., 2002b. Pervasive mantle plume head heterogeneity: evidence from the late Cretaceous Caribbean-Colombian oceanic plateau. Journal of Geophysical Research - Solid Earth 107, B7.
Lee, C.T.A., Luffi, P., Plank, T., Dalton, H., Leeman, W.P., 2009. Constraints on the depths and temperatures of basaltic magma generation on Earth and other terrestrial planets using new thermobarometers for mafic magmas. Earth and Planetary Science Letters 279 (1–2), 20–33.
Madsen, J.K., Thorkelson, D.J., Friedman, R.M., Marshall, D.D., 2006. Cenozoic to Recent plate configurations in the Pacific Basin: ridge subduction and slab window magmatism in western North America. Geosphere 2 (1):11–34. http://dx.doi.org/10.1130/GES00020.1.
Mahoney, J.J., Storey, M., Duncan, R.A., Spencer, K.J., Pringle, M., 1993a. Geochemistry and age of the Ontong Java plateau. In: Pringle, M.S. (Ed.), The Mesozoic Pacific: Geology, Tectonics and VolcanismVolume Geophysical Monograph 77. American Geophysical Union, pp. 233–261.
Mahoney, J.J., Storey, M., Duncan, R.A., Spencer, K.J., Pringle, M., 1993b. Geochemistry and geochronology of Leg 130 basement lavas: nature and origin of the Ontong Java Plateau. In: Berger, W.H., Kroenke, L.W., Mayer, L.A. (Eds.), Proceedings of the Ocean Drilling Program, Scientific Results, Volume 130: College Station, TX, Ocean Drilling Program. Texas A&M University, pp. 3–22.
Mahoney, J.J., Fitton, J.G., Wallace, P.J., et al., 2001. Proceedings of the Ocean Drilling Program, Initial Reports, College Station, Texas, Ocean Drilling Program. pp. 1–75.
Massey, N.W.D., 1986. Metchosin Igneous Complex, southern Vancouver Island - ophiolite stratigraphy developed in an emergent island setting. Geology 14 (7), 602–605.
McCrory, P.A., Wilson, D.S., 2013. A kinematic model for the formation of the Siletz-Crescent forearc terrane by capture of coherent fragments of the Farallon and Resurrection plates. Tectonics 32 (3), 718–736.
McDonald, I., Viljoen, K.S., 2006. Platinum-group element geochemistry of mantle eclogites: a reconnaissance study of xenoliths from the Orapa kimberlite, Botswana. Applied Earth Science: Transactions of the Institutions of Mining and Metallurgy: Section B 115, 81–93.
McLaughlin, R.J., 2009. The Wheatfield Fork terrane: a remnant of Siletzia in Franciscan Complex Coastal Belt of northern California. Proceedings 2009 Portland GSA Annual Meeting 2009.
Moghadam, H.S., Stern, R.J., Rahgoshay, M., 2010. The Dehshir ophiolite (central Iran): geochemical constraints on the origin and evolution of the Inner Zagros ophiolite belt. Geological Society of America Bulletin http://dx.doi.org/10.1130/B30066.1.
Mullen, E.K., Weis, D., 2013. Sr-Nd-Hf-Pb isotope and trace element evidence for the origin of alkalic basalts in the Garibaldi Belt, northern Cascade arc. Geochemistry, Geophysics, Geosystems 14 (8):3126–3155. http://dx.doi.org/10.1002/ggge.20191.

Müller, R.D., Royer, J.-Y., Lawver, L.A., 1993. Revised plate motions relative to the hotspots from combined Atlantic and Indian Ocean hotspot tracks. Geology 21 (3), 275–278.
Nobre Silva, I.G., Weis, D., Barling, J., Scoates, J.S., 2009. Leaching systematics and matrix elimination for the determination of high-precision Pb isotope compositions of ocean island basalts. Geochemistry, Geophysics, Geosystems 10:8. http://dx.doi.org/10.1029/2009GC002537.
Nobre Silva, I.G., Weis, D., Scoates, J.S., 2010. Effects of acid leaching on the Sr-Nd-Hf isotopic compositions of ocean island basalts. Geochemistry, Geophysics, Geosystems 11 (9). http://dx.doi.org/10.1029/2010GC003176.
Nobre Silva, I.G., Weis, D., Scoates, J.S., 2013. Isotopic systematics of the early Mauna Kea shield phase and insight into the deep mantle beneath the Pacific Ocean. Geochemistry, Geophysics, Geosystems 14 (3):659–676. http://dx.doi.org/10.1002/ggge.20047.
O'Neill, C., Muller, D., Steinberger, B., 2005. On the uncertainties in hot spot reconstructions and the significance of moving hot spot reference frames - art. no. Q04003. Geochemistry, Geophysics, Geosystems 6:4003. http://dx.doi.org/10.1029/2004GC000784.
Parsons, T., Wells, R.E., Fisher, M.A., Flueh, E., ten Brink, U.S., 1999. Three-dimensional velocity structure of Siletzia and other accreted terranes in the Cascadia forearc of Washington. Journal of Geophysical Research - Solid Earth 104 (B8), 18015–18039.
Pearce, J.A., 1996. A user's guide to basalt discrimination diagrams. In: Wyman, D.A. (Ed.), Trace Element Geochemistry of Volcanic Rocks: Applications for Massive Sulphide Exploration. Volume Geological Association of Canada, Short Course Notes vol. 12, pp. 79–113.
Pearce, J.A., 2008. Geochemical fingerprinting of oceanic basalts with applications to ophiolite classification and the search for Archean oceanic crust. Lithos 100 (1), 14–48.
Pyle, D.G., Duncan, R.A., Wells, R.E., Graham, D.W., Harrison, B., Hanan, B., 2009. Siletzia: an oceanic large igneous province in the Pacific Northwest. Proceedings 2009 Portland GSA Annual Meeting 2009.
Salters, V.J., Mallick, S., Hart, S.R., Langmuir, C.E., Stracke, A., 2011. Domains of depleted mantle: new evidence from hafnium and neodymium isotopes. Geochemistry, Geophysics, Geosystems 12:8. http://dx.doi.org/10.1029/2011GC003617.
Seton, M., Müller, R.D., Zahirovic, S., Gaina, C., Torsvik, T., Shephard, G., Talsma, A., Gurnis, M., Turner, M., Maus, S., Chandler, M., 2012. Global continental and ocean basin reconstructions since 200 Ma. Earth-Science Reviews 113 (3–4), 212–270.
Snavely, P.D., Wagner, H.C., Lander, D.L., 1980. Interpretation of the Cenozoic geologic history, central Oregon continental margin: Cross-section summary. Geological Society of America Bulletin 91 (3), 143–146.
Snavely, P.D., MacLeod, N.S., Wagner, H.C., 1968. Tholeiitic and alkalic basalts of the Eocene Siletz River volcanics, Oregon coast range. American Journal of Science 266 (6), 454–481.
Stern, R.J., 2004. Subduction initiation: spontaneous and induced. Earth and Planetary Science Letters 226 (3–4), 275–292.
Stern, R.J., Scholl, D.W., 2010. Yin and yang of continental crust creation and destruction by plate tectonic processes. International Geology Review 52 (1), 1–31.
Stracke, A., 2012. Earth's heterogeneous mantle: a product of convection-driven interaction between crust and mantle. Chemical Geology 330, 274–299.
Sun, S., McDonough, W.F., 1989. Chemical and isotope systematics of oceanic basalts: implications for mantle composition and processes. In: Saunders, A.D., Norry, M.J. (Eds.), Magmatism in the Ocean Basins. Geological Society of London, Special Publication vol. 42, pp. 313–345.
Tanaka, R., Nakamura, E., Takahashi, E., 2002. Geochemical Evolution of Koolau Volcano, Hawaii. Hawaiian Volcanoes. Deep Underwater Perspectives. pp. 311–332.
Tejada, M.L.G., Mahoney, J.J., Neal, C.R., Duncan, R.A., Petterson, M.G., 2002. Basement geochemistry and geochronology of central Malaita, Solomon islands, with implications for the origin and evolution of the Ontong Java Plateau. Journal of Petrology 43 (3), 449–484.
Tejada, M.L.G., Mahoney, J.J., Castillo, P.R., Ingle, S.P., Sheth, H.C., Weis, D., 2004. Pin-pricking the elephant: evidence on the origin of the Ontong Java Plateau from Pb-Sr-Hf-Nd isotopic characteristics of ODP Leg 192 basalts. In: Fitton, J.G., Mahoney, J.J., Wallace, P.J., Saunders, A.D. (Eds.), Origin and Evolution of the Ontong Java Plateau. Geological Society of London, Special Publication vol. 229, pp. 133–150.
Tetreault, J., Buiter, S., 2014. Future accreted terranes: a compilation of island arcs, oceanic plateaus, submarine ridges, seamounts, and continental fragments. Solid Earth 5 (2), 243.
Thompson, P.M.E., Kempton, P.D., White, R.V., Saunders, A.D., Kerr, A.C., Tarney, J., Pringle, M.S., 2004. Elemental, Hf-Nd isotopic and geochronological constraints on an island arc sequence associated with the Cretaceous Caribbean plateau: Bonaire, Dutch Antilles. Lithos 74 (1–2), 91–116.
Trehu, A.M., Asudeh, I., Brocher, T.M., Luetgert, J.H., Mooney, W.D., Nabelek, J.L., Nakamura, Y., 1994. Crustal architecture of the Cascadia fore-arc. Science 266 (5183), 237–243.
Weaver, B.L., 1991. The origin of ocean island basalt end-member compositions: trace element and isotopic constraints. Earth and Planetary Science Letters 104, 381–397.
Weis, D., Frey, F.A., 2002. Submarine basalts of the northern Kerguelen Plateau: Interaction between the Kerguelen Plume and the Southeast Indian Ridge revealed at ODP Site 1140. Journal of Petrology 43 (7), 1287–1309.
Weis, D., Frey, F.A., Schlich, R., Schaming, M., Montigny, R., Damasceno, D., Mattielli, N., Nicolaysen, K.E., Scoates, J.S., 2002. Trace of the Kerguelen mantle plume: evidence from seamounts between the Kerguelen Archipelago and Heard Island, Indian Ocean. Geochemistry, Geophysics, Geosystems 3:6. http://dx.doi.org/10.1029/2001GC000251.
Weis, D., Kieffer, B., Maerschalk, C., Barling, J., de Jong, J., Williams, G.A., Hanano, D., Pretorius, W., Mattielli, N., Scoates, J.S., 2006. High-precision isotopic characterization of USGS reference materials by TIMS and MC-ICP-MS. Geochemistry, Geophysics, Geosystems 7:8. http://dx.doi.org/10.1029/2006GC001283.
Weis, D., Kieffer, B., Hanano, D., Nobre Silva, I., Barling, J., Pretorius, W., Maerschalk, C., Mattielli, N., 2007. Hf isotope compositions of US geological survey reference materials. Geochemistry, Geophysics, Geosystems 8:6. http://dx.doi.org/10.1029/2006GC001473.
Weis, D., Garcia, M.O., Rhodes, J.M., Jellinek, M., Scoates, J.S., 2011. Role of the deep mantle in generating the compositional asymmetry of the Hawaiian mantle plume. Nature Geoscience 4 (12), 831–838.
Wells, R., Engebretson, D., Snavely, P., Coe, R., 1984. Cenozoic plate motions and the volcano-tectonic evolution of western Oregon and Washington. Tectonics 3 (2), 275–294.
Wells, R.E., Weaver, C.S., Blakely, R.J., 1998. Fore-arc migration in Cascadia and its neotectonic significance. Geology 26 (8), 759–762.
Wells, R.E., Jayko, A.S., Niem, A., Black, G.L., Wiley, T.J., Baldwin, E., Molenaar, K., Wheeler, K., DuRoss, C., Givler, R., 2000. Geologic Map and Database of the Roseburg 30 × 60 Quadrangle, Douglas and Coos Counties, Oregon, US Department of the Interior, US Geological Survey Open-File Report 00-376.
Wells, R., Bukry, D., Friedman, R., Pyle, D., Duncan, R., Haeussler, P., Wooden, J., 2014. Geologic history of Siletzia, a large igneous province in the Oregon and Washington Coast Range: correlation to the geomagnetic polarity time scale and implications for a long-lived Yellowstone hotspot. Geosphere 10 (4):692–719. http://dx.doi.org/10.1130/GES01018.1.
Whattam, S.A., Stern, R.J., 2011. The 'subduction initiation rule': a key for linking ophiolites, intra-oceanic forearcs, and subduction initiation. Contributions to Mineralogy and Petrology 162 (5), 1031–1045.
White, W.M., Patchett, P.J., 1984. Hf-Nd-Sr isotopes and incompatible element abundances in island arcs: implications for magma origins and crust–mantle evolution. Earth and Planetary Science Letters 67, 167–185.
Wolff, J., Ramos, F., Hart, G., Patterson, J., Brandon, A., 2008. Columbia River flood basalts from a centralized crustal magmatic system. Nature Geoscience 1 (3), 177–180.
Workman, R.K., Hart, S.R., Jackson, M., Regelous, M., Farley, K.A., Blusztajn, J., Kurz, M., Staudigel, H., 2004. Recycled metasomatized lithosphere as the origin of the enriched mantle II (EM2) end-member: evidence from the Samoan volcanic chain. Geochemistry, Geophysics, Geosystems 5. http://dx.doi.org/10.1029/2003GC000623.
Yorath, C.J., Sutherland Brown, A., Massey, N.W.D., 1999. Lithoprobe, Southern Vancouver Island, British Columbia: Geology. With contributions by TDJ England, RM Bustin, Ottawa. http://dx.doi.org/10.4095/210350.